ORIGINAL RESEARCH Open access

Multi-Temporal Sentinel-2 and UAV Data Fusion for Improved Vineyard Monitoring and Management

Grace Wanjiru*, James Mwangi[1], Samuel Kiprop[2], Cynthia Atieno[3], Peter Odhiambo[4]

Abstract

The growing reliance on geospatial data from satellites and unmanned aerial vehicles (UAVs) has driven significant expansion in the range of tools and techniques for data collection and processing. Effective vineyard (and most crop) management requires reliable access to spatial and temporal variability. This awareness across the full vegetative cycle of any crop is essential for achieving greater efficiency, particularly in viticulture. Numerous studies conducted over recent years have leveraged satellite and UAV data—applied either separately or jointly—to support crop management goals. Still, few investigations have addressed the multi-temporal integration of these two data sources, whether independently or in synergy. The present work seeks to pinpoint the optimal data sources and approaches for adoption at precise points in the vineyard phenological cycle. Sentinel-2 data drawn from two vineyard plots in the Douro Demarcated Region (Portugal) were evaluated against UAV multi-spectral data across three distinct conditions: the full vineyard plot; solely the grapevine canopy; and inter-row zones (with all grapevine vegetation removed). Outcomes reveal that both platforms successfully capture vineyard variability throughout the growth period, though with differing levels of granularity. Sentinel-2 data are suitable for mapping soil variability in vineyards, whereas the enhanced spatial resolution of UAV-based data enables broader applications. Overall, each data type, when used alone, can supply meaningful insights for vineyard management depending on the specific objective.

Keywords Unmanned aerial vehicles, Sentinel-2, Vitis vinifera, Grapevine phenology, Multi-temporal monitoring, Douro demarcated region

*Correspondence:
Grace Wanjiru
grace.wanjiru@uonbi.ac.ke
[1] Department of AI for Maize Lethal Necrosis Disease Detection using UAV Multispectral Data, Faculty of Agriculture, University of Nairobi, Nairobi, Kenya
[2] Department of Smart Weather-Based Pest Warning Systems, Faculty of Agriculture, Moi University, Eldoret, Kenya
[3] Department of Machine Learning for Soil Nutrient Depletion Prediction, Faculty of Agriculture, Kenyatta University, Nairobi, Kenya
[4] Department of Precision Fertilizer Recommendation for Smallholder Farms, Faculty of Agriculture, Egerton University, Njoro, Kenya

Introduction

Precision Agriculture (PA) emerged as a method to refine inputs and farming practices to reduce the unevenness across agricultural fields [1]. This concept ties directly to the five “R”s principle, which emphasizes delivering the right product, at the right time, in the right place, in the right manner, and in the right quantity [2]. Application of PA methods within viticulture—often termed precision viticulture (PV)—remains a fairly recent development [3]. PV primarily strives for sustainable output by reducing and optimizing energy, fertilizer, chemical, and other resource consumption, thereby decreasing costs while enhancing oversight of quality and productivity [4].

Optimizing resources and overseeing production activities becomes feasible through continuous assessment of variability across an agricultural zone via remote [5] or proximal [6] sensing methods that facilitate sound crop handling [7]. Remote

This is an open access article distributed under the terms of the Creative Commons Attribution-NonCommercial-ShareAlike 4.0 International License (CC BY-NC-SA 4.0), which permits non-commercial use, distribution, reproduction, and adaptation in any medium or format, provided that appropriate credit is given to the original author(s) and source, a link to the license is provided, and any changes made are indicated. Adapted material must be distributed under the same license.

© 2026 The Author(s). | Published by Agro Intelligence Research Press

sensing is widely adopted in agriculture thanks to its adaptability [5]. Sensors on these platforms capture information from multiple regions of the electromagnetic spectrum at varying spatial and temporal scales [8]. In PV, spatial resolution is a critical factor in remote sensing because it strongly influences the ability to separate canopy structure or vineyard heterogeneity [9]. Although spaceborne systems face certain constraints (such as cloud interference [10] and limited scheduling flexibility [11]), satellites have grown increasingly important in agronomy [12] due to better spatial resolution and greater data accessibility [13].

Advancements in technology have spurred major progress in remote sensing, notably through the rise of unmanned aerial vehicles (UAVs). These platforms enable rapid, cost-effective field data collection [14]. By operating close to the surface, UAVs achieve finer spatial resolution [13] and experience minimal cloud disruption. Their adaptability also covers sensor choice, observation angles, resolution levels, and revisit frequency [11]. The chief drawback remains their limited coverage of expansive territories [15], making them best suited for small- to medium-scale efforts [4]. This flexibility particularly strengthens temporal resolution, supporting repeated tracking of shifts in vegetation and soil features [16]. In practice, the majority of UAV crop monitoring relies on vegetation indices (VIs) calculated through mathematical combinations of multiple spectral bands [17]. These indices help observe, evaluate, and map differences in plant architecture [7] along with associated biophysical traits [18]. In the field of PV, over 90 such VIs have already seen application [19].

Among these, the Normalized Difference Vegetation Index (NDVI) [20] ranks among the strongest tools for remotely observing vegetation development and status [21]. Dense, vigorous canopies reflect little in the red spectrum while reflecting strongly in the near-infrared (NIR) spectrum, yielding positive NDVI readings [22]. Within PV, NDVI has demonstrated value in revealing seasonal differences in grapevine vigor and yield [23, 24], spotting vine damage [25], measuring heat stress [26], and guiding variable-rate fertilizer programs [27, 28]. Such benefits depend on collecting data at well-chosen moments during the crop's phenological development.

Accurately tracking phenological shifts in grapevines and determining plant health status requires NDVI computation from imagery with appropriate revisit frequency. Medium-resolution satellite data, exemplified by Copernicus Sentinel-2, offers broad vegetation insights [29] and supports vigor mapping plus large-area oversight [30]. Yet Sentinel-2 multi-spectral imagery may have limited value for small or patchy areas with mixed soil and vegetation [29, 30], especially where grapevine canopy coverage is below 25% [7]. Pathways, grasses, and shrubs in inter-row spaces can further distort assessments of crop condition [31]. Deeper insight into soil–plant dynamics and their temporal evolution demands more precise techniques [32] capable of detailed characterization of surface elements [26]. UAV-mounted high-resolution multi-spectral sensors help overcome these constraints.

Comparative analyses of Sentinel-2 and UAV multi-spectral imagery in vineyards have identified notable variations in both row [29, 31] and trellis [33] training systems, with Sentinel-2 performing particularly well in the latter. Parallel work exists for other crops, including pastures [34], onions [35], and sugarcane [36]. Nevertheless, available publications tend to examine grapevine variability only during limited phenological windows, such as flowering through ripening [29], berry ripening [7], or harvest [37]. Comprehensive evaluations spanning the entire reproductive cycle [24, 31] (from budbreak to harvest) remain scarce. In essence, current literature focuses on platform comparisons for isolated cycle segments, highlighting observed shifts and weighing platform strengths and limitations. General agreement holds that medium-resolution data is suitable for large zones [27, 29], as it captures major changes during the reproductive phase and aids routine field operations [33]. Further examination is warranted to assess whether such satellites can detect meaningful grapevine changes in row-trained systems during vegetative growth and to explore genuine UAV–satellite integration. Alvarez-Vanhard *et al.* [11] noted valuable synergies that remain underused; current practice remains anchored in "UAV or Satellite" or "UAV for Satellite" thinking. The authors advocate advancing toward a complementary "UAV and Satellite" model.

In this context, the current study aims to clarify during which portions of the vineyard vegetative cycle Sentinel-2 multi-spectral data can deliver sufficient detail for efficient plot-level management. Two time-series datasets (Sentinel-2 and

© 2026 The Author(s). | Published by Agro Intelligence Research Press

UAV multi-spectral) were assembled, covering key vegetative phases in two plots within the Douro winemaking region of northern Portugal. The work seeks to delineate periods in which Sentinel-2 data alone suffices, stages requiring UAV data exclusively, and phases in which both sources can operate effectively together. These insights prove especially relevant for regions relying on small, traditional vineyard plots that lack modern management support technologies—a common reality across many Mediterranean areas.

Materials and Methods

Study area

The research was conducted in vineyards near Vila Real, Portugal, within the Douro Demarcated Region (DDR) **(Figure 1b)**. Coordinates span 41°17′41.64″ N to 7°42′59.53″ W (World Geodetic System 1984-WGS84). The total studied surface area measures roughly 2 hectares, split into two 1-hectare plots: Plot A (cv. Sousão) and Plot B (cv. Sauvignon blanc) **(Figure 1c)**. Vines follow the Cordon Royat training system, managed for moderate vegetative vigor. Within rows, plants are spaced 1 m apart, while the inter-row distance is 2 m. Altogether, 45 rows oriented N–S were included. Inter-row spaces contain natural vegetation, with mechanical management applied at least twice yearly. The vineyard operates under rainfed conditions, receives foliar fertilization, and undergoes phytosanitary treatments across the full season.

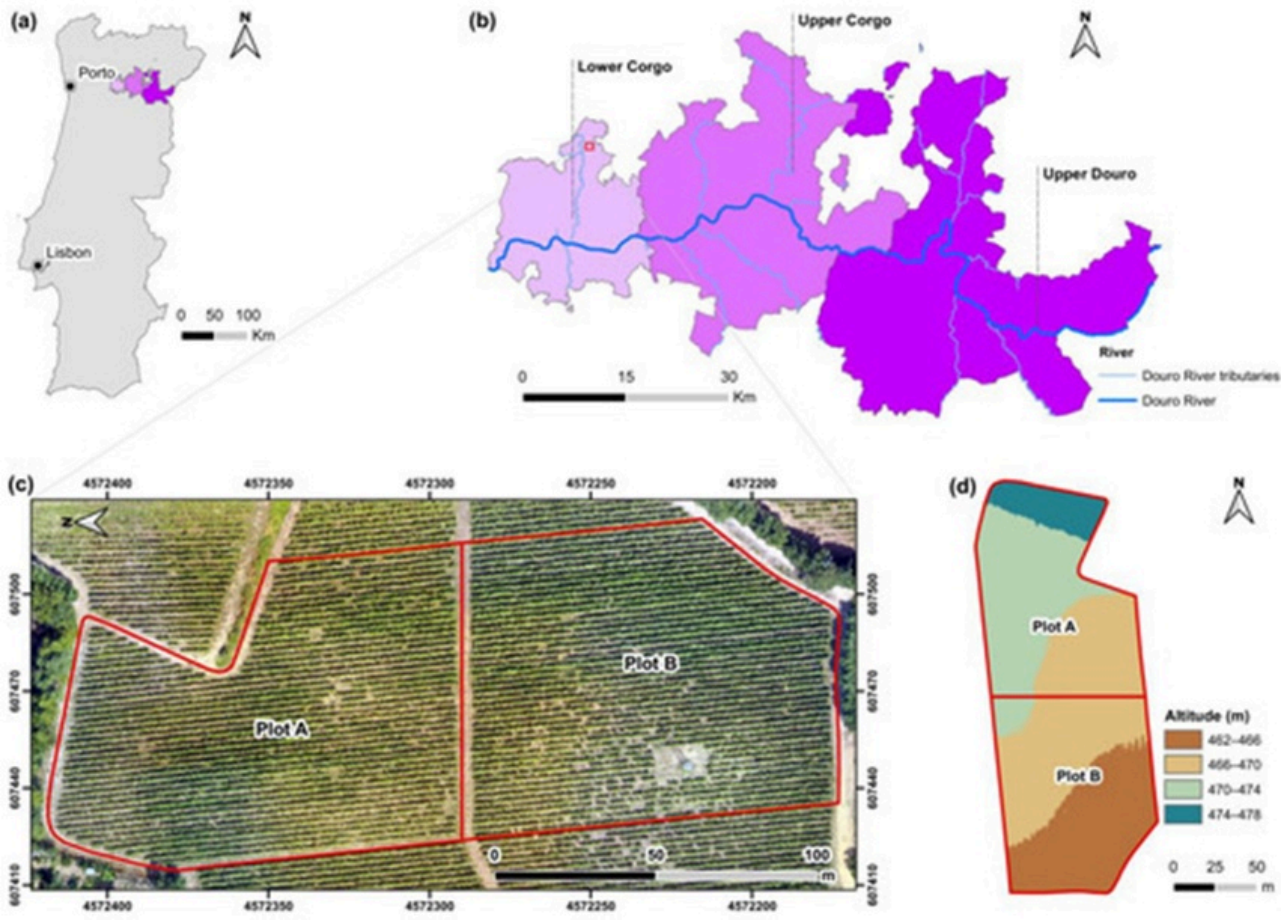


Figure 1. Study area presentation: location of the study area in the Douro Demarcated Region (RDD), northern Portugal (a, b); (c) overview of the study area and its digital terrain model (d). The plots' boundaries are delimited by red lines. Coordinates are in World Geodetic System 1984, Universal Transverse Mercator (UTM), zone 29 N (EPSG: 32629).

© 2026 The Author(s). | Published by Agro Intelligence Research Press

The south-facing vineyard occupies mostly level terrain. Plot A ranges in elevation from 467 to 478 m, while Plot B lies between 462 and 471 m **(Figure 1d)**. Terrain and soil irregularities produce noticeable differences in vigor both within and across plots. Over the observation window (April to September 2021), accumulated precipitation reached 350 mm—equivalent to 35% of the annual total of 991 mm—paired with 827 mm of evapotranspiration. The average maximum, mean, and minimum temperatures were 27.88 °C, 13.80 °C, and 2.77 °C, respectively. Monthly patterns appear in **Figure 2**. Data originated from a weather station (iMETOS, Pessl Instruments GmbH, Weiz, Austria) positioned 200 m from the site. Peak temperatures occurred in July, August, and September, while January, February, and December recorded the highest rainfall. March, July, and August showed virtually no precipitation.

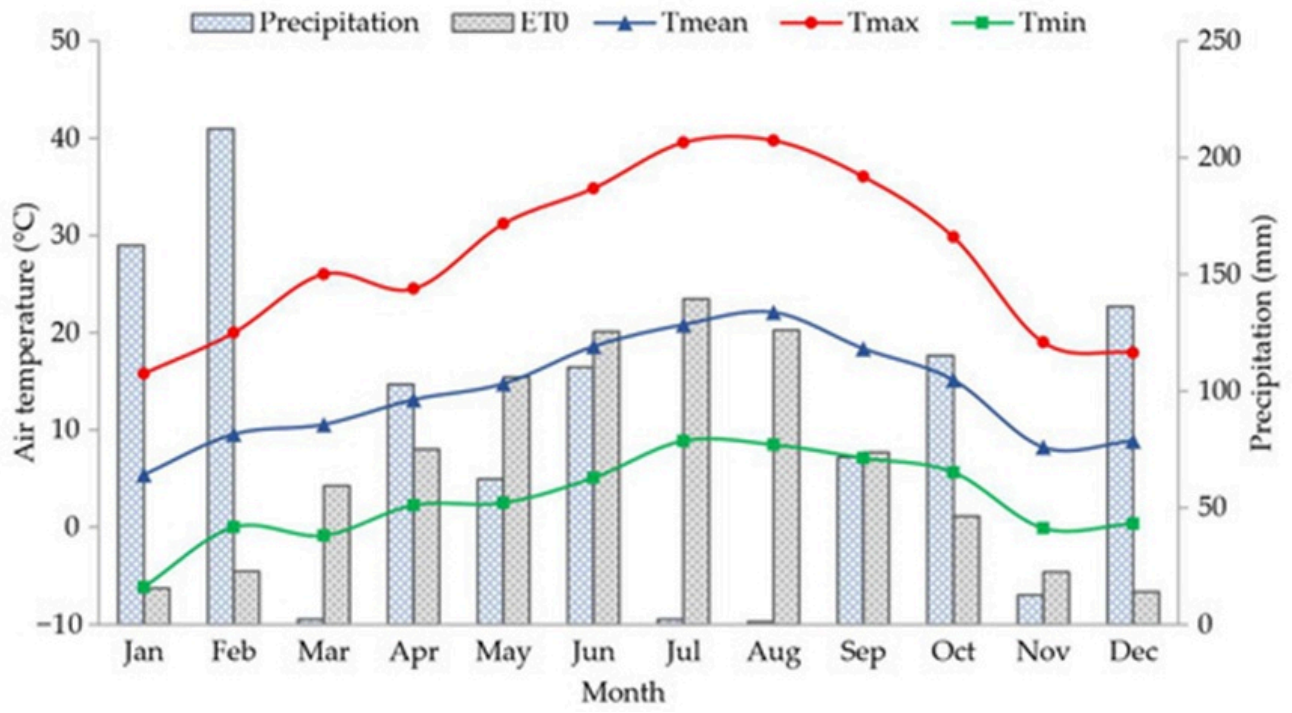


Figure 2. Monthly maximum (Tmax), mean (Tmean), and minimum (Tmin) air temperature; precipitation totals and evapotranspiration (ET0) of the studied area in the year 2021.

Remote-sensed data

Multi-spectral records for this investigation were obtained from two separate remote sensing systems, Sentinel-2 and UAV, during the 2021 growth period. Collections were conducted on six occasions from April to September **(Table 1)**, spanning several grapevine vegetative phases.

Table 1. Acquisition dates of Sentinel-2 and unmanned aerial vehicle (UAV) data and the temporal difference between them for each analyzed period, the corresponding grapevine growth stages, and their BBCH codes [38] in each plot, where each growth stage corresponds to: 1—leaf development; 5—inflorescence emergence; 6—flowering; 7—development of fruits; and 8—ripening of berries.

Period	Acquisition date	Data source	Difference (Days)	Growth stage	BBCH code
April	30 April 2021	UAV	4	1 (both plots)	13 (plot A), 16 (plot B)
April	4 May 2021	Sentinel-2			
May	25 May 2021	UAV	4	5 (both plots)	55 (plot A), 57 (plot B)

© 2026 The Author(s). | Published by Agro Intelligence Research Press

May	29 May 2021	Sentinel-2			
June	11 June 2021	UAV	3	6 (both plots)	68 (plot A), 69 (plot B)
June	8 June 2021	Sentinel-2			
July	13 July 2021	UAV	0	7 (both plots)	71 (plot A), 73 (plot B)
July	13 July 2021	Sentinel-2			
August	4 August 2021	UAV	7	7 (plot A), 8 (plot B)	79 (plot A), 81 (plot B)
August	28 July 2021	Sentinel-2			
September	15 September 2021	UAV	6	8 (both plots)	85 (plot A), 89 (plot B)
September	21 September 2021	Sentinel-2			

Sentinel-2

The Sentinel-2 multi-spectral instrument (MSI) gathers information in 13 segments of the electromagnetic spectrum, covering visible, NIR, and short-wave infrared (SWIR) ranges. It delivers spatial resolutions of 10 m, 20 m, and 60 m, features a five-day revisit frequency, and covers 100 × 100 km per tile [39]. Cloud-free Level-2A Sentinel-2 Bottom of Atmosphere (BOA) reflectance images served this work. Level-2A involves scene classification plus atmospheric correction performed on Level-1C ortho-image Top of Atmosphere (TOA) products [40]. Only the red and NIR bands (Bands 4 and 8) were used here for VI calculation. Sentinel-2 tiles were acquired on dates aligned as closely as possible with UAV flight timing to minimize major inconsistencies when judging vineyard vegetative condition.

Unmanned aerial vehicle

High-resolution RGB and multi-spectral aerial images were captured with the Phantom 4 (DJI, Shenzhen, China). The native Phantom 4 camera, fixed on a 3-axis gimbal (FCC 3 model, 12.4 megapixels), supplied RGB imagery. Multi-spectral capture relied on the Parrot SEQUOIA sensor (Parrot SA, Paris, France) for green, red, red edge, and NIR bands at 1.2 MP resolution.

UAV missions aligned with key phenological phases on the Biologische Bundesanstalt, Bundessortenamt, und CHemische Industrie (BBCH) scale [38]. Flights ran from leaf development (three unfolded leaves, April) through berry ripening (ready for harvest, September), with additional information in **Table 1**. Imagery collection took place near solar noon to minimize shadow impacts, under clear skies and calm winds, at 50 m altitude, with 80% forward and 70% side overlap.

Ground sampling distance (GSD) was measured at about 0.02 m for RGB imagery and 0.05 m for multi-spectral imagery. Radiometric calibration included photographing a manufacturer-provided reflectance panel (Airinov, Paris, France) before each flight, along with irradiance readings from the UAV's top-mounted sunlight sensor. This setup ensured a robust radiometric process for consistent reflectance values across flights, dates, and weather conditions.

Phenological modeling

Growing degree-day (GDD) calculations provided reliable information on vineyard development. Although advanced indices exist, GDD functions as a basic yet globally recognized measure. Air temperature inputs allowed GDD computation from 1 January to 30 October 2021 via the Winkler Equation [41-43], commonly written as in **Eq. 1**:

$$GDD\ (t) = \sum_{t=0}^{t} \left[\frac{T_{max} + T_{min}}{2} \right] - T_{base} \quad (1)$$

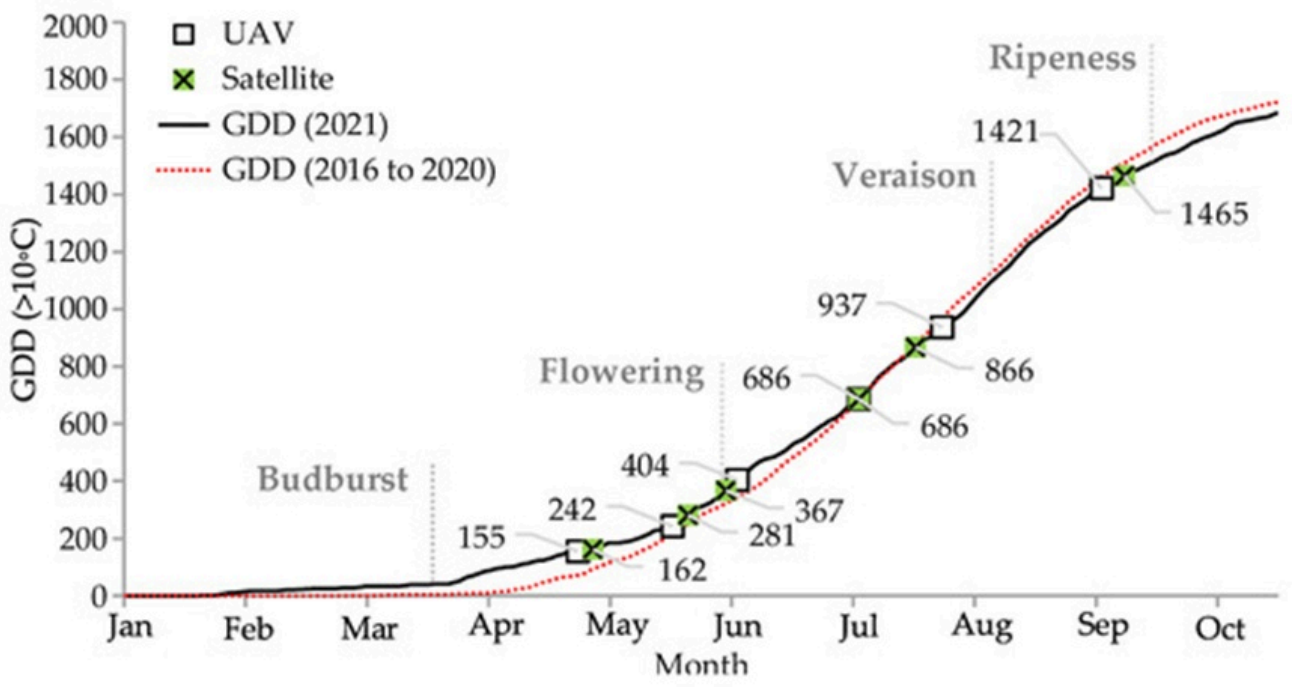
© 2026 The Author(s). | Published by Agro Intelligence Research Press

Where t is the number of days from the starting date of GDD calculation (1 January), Tmax is the daily maximum air temperature, Tmin is the daily minimum air temperature, and Tbase is the reference base temperature, below which the process of interest does not progress. Tbase varies among species, possibly among cultivars, and probably with the phase or growth stage under consideration [41]. For this study, a Tbase value of 10 °C was used, corresponding to vegetative zero for grapevines [42]. The vineyard phenology was defined based on GDD and corroborated the BBCH scale [43, 44] and was monitored weekly. To proceed with the analysis of the different grapevine phenological stages, six UAV and Satellite data acquisitions were carried out from April to September 2021 **(Figure 3)**. The data collected covered the main crop stages of the grapevine, starting with leaf development (tree leaves unfolded) and including inflorescence emergence, flowering, fruit development, and berry ripening (berries ripe for harvest).



Figure 3. Photographic details of the vineyard plots (Plots A and B) for the data acquisition period and the grapevine phenological stages according to the extended BBCH scheme [38].

GDD values for 2021 at the research site, along with those from the prior four years, are shown in **Figure 4**. Heat accumulation per interval for both remote sensing systems is also shown. Field-observed key phenological phases matched findings from other work on cv. Sauvignon blanc [45] and cv. Sousão [46].



© 2026 The Author(s). | Published by Agro Intelligence Research Press

Figure 4. Growing degree days (GDD) for the monitored vineyard plots were calculated from 1 January 2021 to 30 October 2021. The average GDD accumulated over the previous four years, with indications of the most relevant phenological stages and data acquisition periods for the two platforms: unmanned aerial vehicle (UAV) and Sentinel-2 (satellite).

Data processing

Each UAV flight campaign's imagery went through processing in Pix4Dmapper Pro version 4.5.6 (Pix4D SA, Lausanne, Switzerland). The software uses structure-from-motion (SfM) methods to locate matching points across images. Initial processing (step 1) calibrates the camera's internal and external settings and computes initial tie points, forming a sparse point cloud. Ground control points (GCPs) were established during this phase to ensure consistency in the outputs of the two sensors (RGB and multi-spectral) over time. Six GCPs covered the area: four positioned near corners and two centrally. Step 2 builds and classifies dense point clouds. The final step generates orthorectified rasters by smoothing and filtering noise in the dense cloud points. Interpolation and orthorectification then yield: (i) RGB orthophoto mosaic; (ii) digital terrain model (DTM); (iii) digital surface model (DSM); and (iv) vegetation indices derived from multi-spectral data.

For thorough review of each plot (Plot A and Plot B) based on UAV multi-spectral radiometric values and comparison against Sentinel-2 MSI data (10 m × 10 m), three UAV data scenarios emerged: (i) full dataset, covering pixels of all vineyard elements (grapevines, inter-row vegetation, bare soil); (ii) grapevine canopy alone, removing every non-grapevine pixel; and (iii) inter-row zones only, using pixels strictly from spaces between rows (all grapevine vegetation removed). QGIS, a geographic information system, handled geospatial work (version 3.22.8, Open Source Geospatial Foundation Project, http://qgis.osgeo.org (accessed on 9 October 2022)). A crop surface model (CSM) first arose from DSM minus DTM subtraction, per **Eq. 2**. RGB-derived digital elevation models fed the CSM. QGIS Raster Calculator produced monthly CSMs (April–September).

$$CSM = DSM - DTM \quad (2)$$

Two series of six masks each were provided by the CSM to outline the grapevine canopy and inter-row zones. Masks targeted pixels above set height levels. Canopy masks excluded soil and inter-row vegetation pixels unrelated to vines: heights over 0.2 m for April–May and over 0.5 m from June onward. Inter-row masks used non-grapevine pixels selected based on local vegetation height per period. **Eq. 3** guided mask creation, separating samples via inclusion rules.

$$Mask = \frac{(CSM\alpha \times 1)}{[(CSM\alpha \times 1) + (CSM\beta \times 0)]} \quad (3)$$

Where α corresponds to the height value of the data set to be filtered, and in front of it is assigned a sign that corresponds to the direction of the order of magnitude (e.g., >, ≥, < or ≤). β refers to the same value assigned to α, but it must be accompanied by the inverse of the magnitude sign. Pixel values of 0 and 1 indicate the absence or presence of information at the end of the process, respectively. From these masks, the three initially proposed scenarios are created by distinguishing the grapevine canopy and inter-row elements. For each mask, the NDVI values are computed from the radiometric information provided by the UAV-based multi-spectral in Pix4Dmapper Pro, as in **Eq. 4**. The assignment of NDVI values to the masks is performed directly in QGIS using the raster calculator, multiplying the mask values by the NDVI for each period (April to September). A visual representation of the computed masks, overlaid on an RGB orthophoto mosaic, is shown in **Figure 5**.

© 2026 The Author(s). | Published by Agro Intelligence Research Press

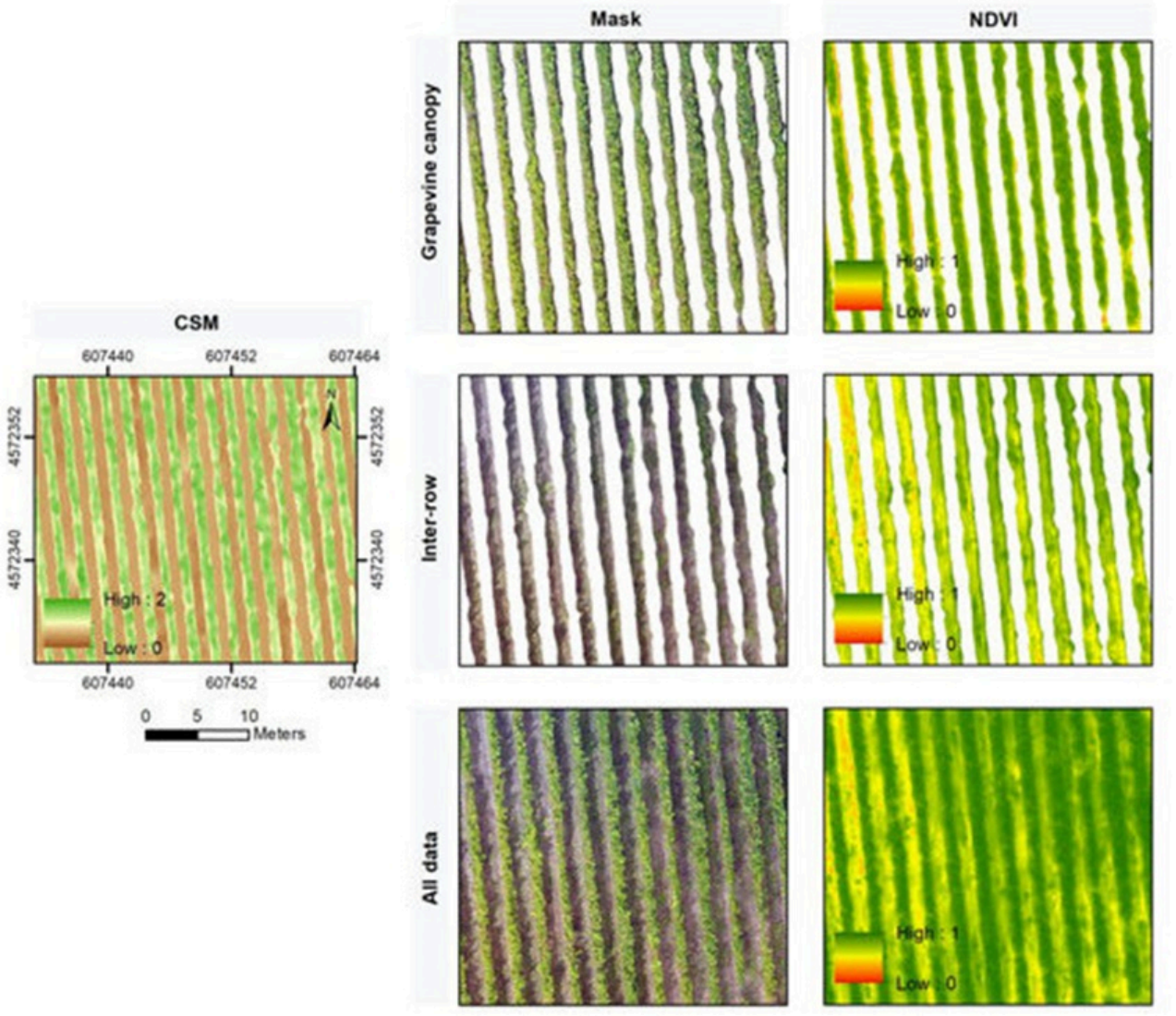


Figure 5. Sequence of operations to establish the different evaluated vineyard scenarios (all data, inter-row, and grapevine canopy). This process is conducted over different periods using crop surface models (CSMs), from which masks are produced, and the corresponding normalized difference vegetation index (NDVI) values are assigned. Coordinates in World Geodetic System 1984, Universal Transverse Mercator (UTM), zone 29 N.

$$NDVI = \frac{NIR - Red}{NIR + Red} \quad (4)$$

UAV-based NDVI relied on roughly 0.02 m pixels **(Figure 6a)**, offering fine detail relative to Sentinel-2 MSI's 10 m resolution. Fair comparison demanded resolution harmonization. A grid sized to Sentinel-2 pixels and positioned accordingly overlaid the plots. The QGIS Zonal Statistics plugin averaged the original pixel NDVI values within each grid cell. UAV NDVI from all data, inter-row, and grapevine canopy scenarios across flights and Sentinel-2 dates received assignment to matching grid cells **(Figure 6b)**. Final processing selected fully internal cells within site boundaries, split by plot, producing 83 cells for Plot A and 80 cells for Plot B **(Figure 6c)**. Plot-level NDVI comparison used averaged values from each UAV scenario and Sentinel-2 pixels per 1 ha plot.

© 2026 The Author(s). | Published by Agro Intelligence Research Press

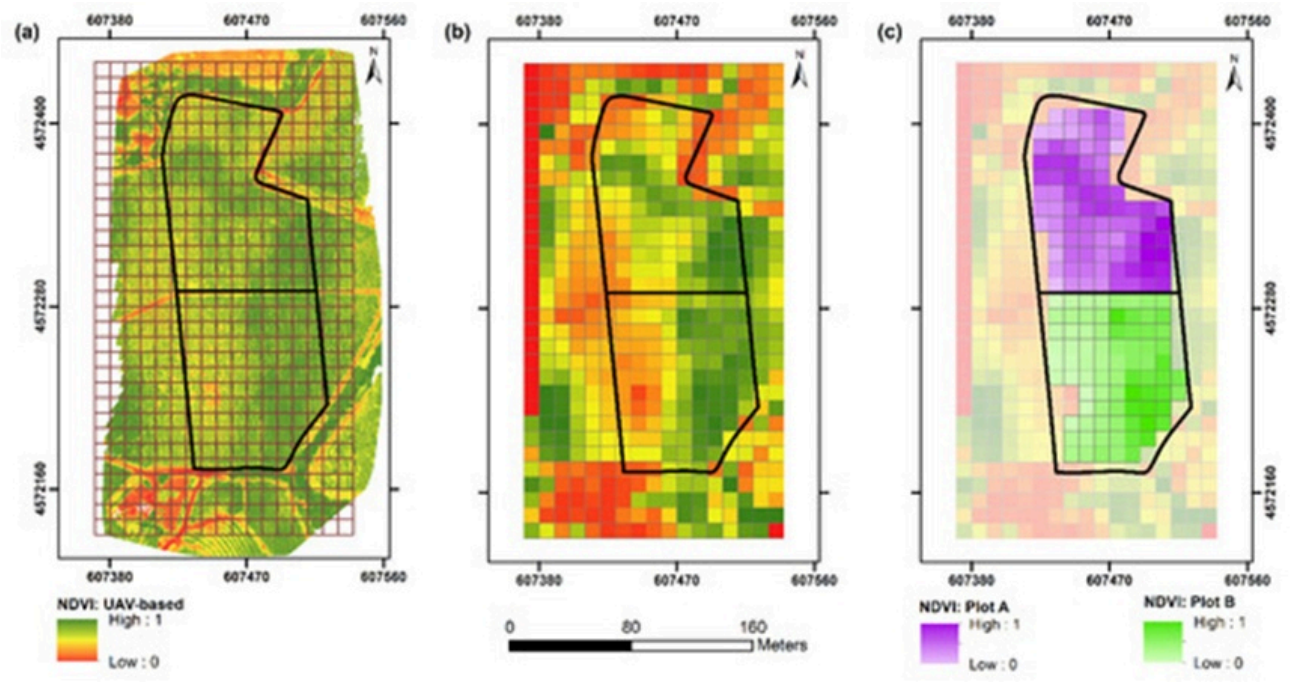


Figure 6. Process to standardize the unmanned aerial vehicle (UAV) data to the Sentinel-2 spatial resolution. The normalized difference vegetation index (NDVI) values for the whole vineyard (a). Mean NDVI value for the set of pixels within each cell (b). Selection of cells inserted within each plot (Plot A and Plot B) (c). Data from the September 2021 flight campaign. Coordinates in World Geodetic System 1984, Universal Transverse Mercator (UTM), zone 29 N (EPSG: 32629).

Masks for grapevines enabled calculation of canopy area plus volume while assessing impacts on satellite NDVI across the growth cycle. Canopy area summed pixels inside every 10 × 10 m cell, then multiplied by individual pixel area (4 × 10−4 m2). Canopy volume applied a 2.5D method [47] multiplying pixel area by height from the CSM. Herbaceous inter-row vegetation's influence on NDVI was also reviewed. A filter-limited inter-row mask NDVI was applied to vigorous plants, yielding values above 0.5 [48], thereby excluding stones, bare soil, and dry material.

Data analysis

NDVI outcomes from each flight mission for the three UAV strategies (full vineyard coverage, grapevine canopy only, and inter-row sections) are compared with Sentinel-2 NDVI readings using common statistical tools. Examination of unique features is performed independently for each plot. Comparisons of NDVI statistics (averages, minimums, maximums, and standard deviations) are also conducted across the three UAV strategies and Sentinel-2 NDVI readings (hereafter referred to as the satellite scenario). Statistical summaries of NDVI values for each scenario are presented as box plots.

One-way ANOVA testing checks whether the independent factors (all data, inter-row, grapevine canopy, satellite) affect the response factor (vigor). The null hypothesis treats all scenarios as identical (H0: x1 = x2 = … = xn) while the alternative claims at least one scenario stands apart (H1: xi ≠ xj = … = xn, for at least one i, j, or n). Application of Tukey's test at the 5% significance level [49] confirms significant differences among scenarios. The statistical relationship between scenarios built from UAV and Sentinel-2 sources is expressed by the coefficient of determination (R2). Furthermore, the average NDVI per method across time is evaluated within both vineyard plots using the tested strategies.

Results and Discussion

© 2026 The Author(s). | Published by Agro Intelligence Research Press

Data characterization

Average NDVI patterns per plot through time under each strategy feature in **Figure 7**. Under the tested conditions, NDVI mirrors vineyard growth patterns, reaching its lowest readings in April and May. By contrast, peak readings occur in July, followed by an overall decline in August and a minor recovery in the harvest window (September). Gaps in average NDVI across strategies remain modest in April and July but widen modestly in May, June, August, and September. The smallest readings occur in inter-row sections, closely matching the all-data pattern. Both plots started with comparable NDVI in April and showed only small gaps among strategies, yet these gaps widened as vineyard growth advanced. In April, the vineyard is in leaf development **(Figure 3)**. At that point, inter-row elements dominated, bringing NDVI readings closer together across all approaches. With further grapevine canopy expansion, especially after August, inter-row influence weakened. Like the UAV inter-row strategy, satellite (Sentinel-2) NDVI readings also sit slightly below overall UAV NDVI readings, particularly in April.

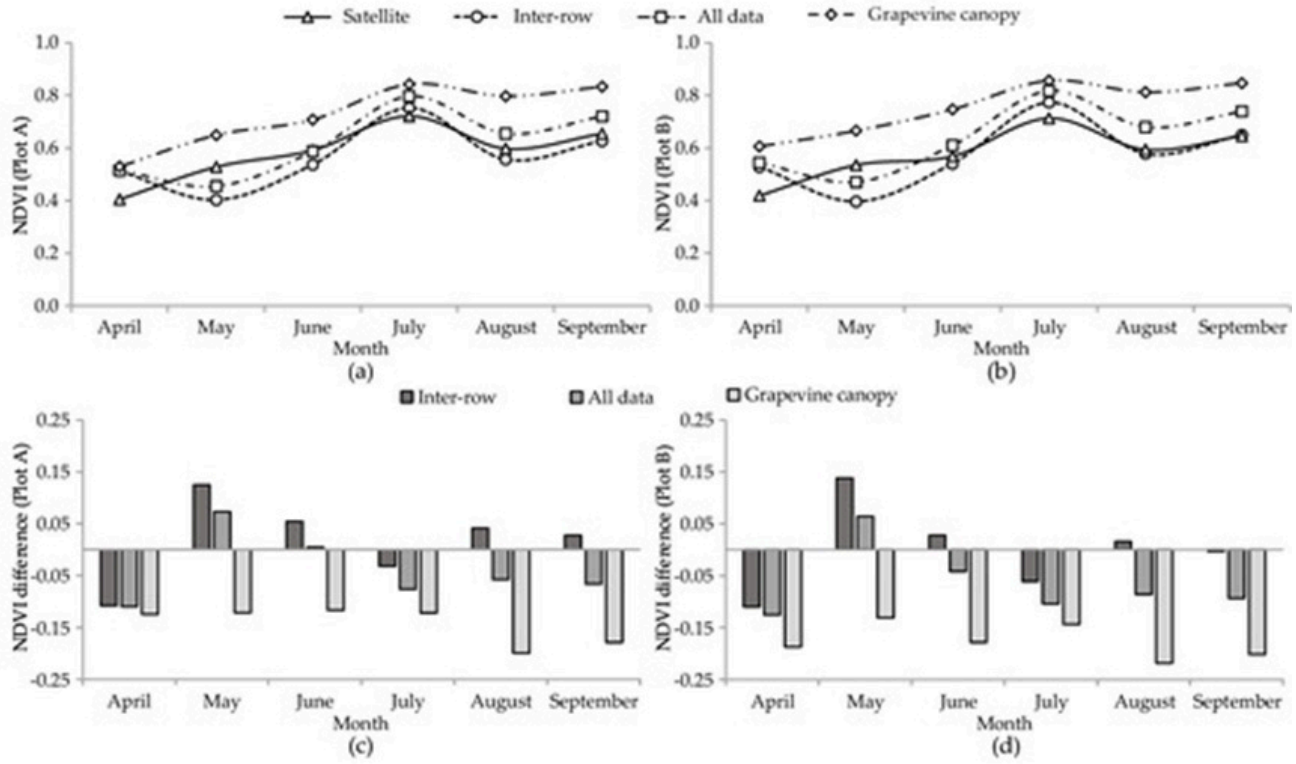


Figure 7. Mean normalized difference vegetation index (NDVI) value in (a) Plot A (cv. Sousão) and (b) Plot B (cv. Sauvignon blanc) in the different evaluated scenarios (all data, inter-row, grapevine canopy, and satellite) for six months (April to September 2021). Difference between the mean NDVI value obtained from Sentinel-2 on Plot A (c) and Plot B (d) compared to the scenarios computed from the unmanned aerial vehicle multi-spectral data.

Although **Figure 7** shows average NDVI at native sensor resolutions, **Figure 8** offers another view, standardized to Sentinel-2 resolution, for straightforward dataset matching. Statistical gaps between scenarios and internal plus cross-plot variability become clear. Both plots follow broadly parallel monthly patterns, starting with reduced NDVI early on. The highest point occurs in July, dips the next month slightly, then climbs again in September. UAV grapevine canopy produced the largest NDVI readings, most obviously in Plot B **(Figure 8b)**. The grapevine canopy dataset also shows a narrower interquartile range, with its median closer to the upper end of the NDVI range.

© 2026 The Author(s). | Published by Agro Intelligence Research Press

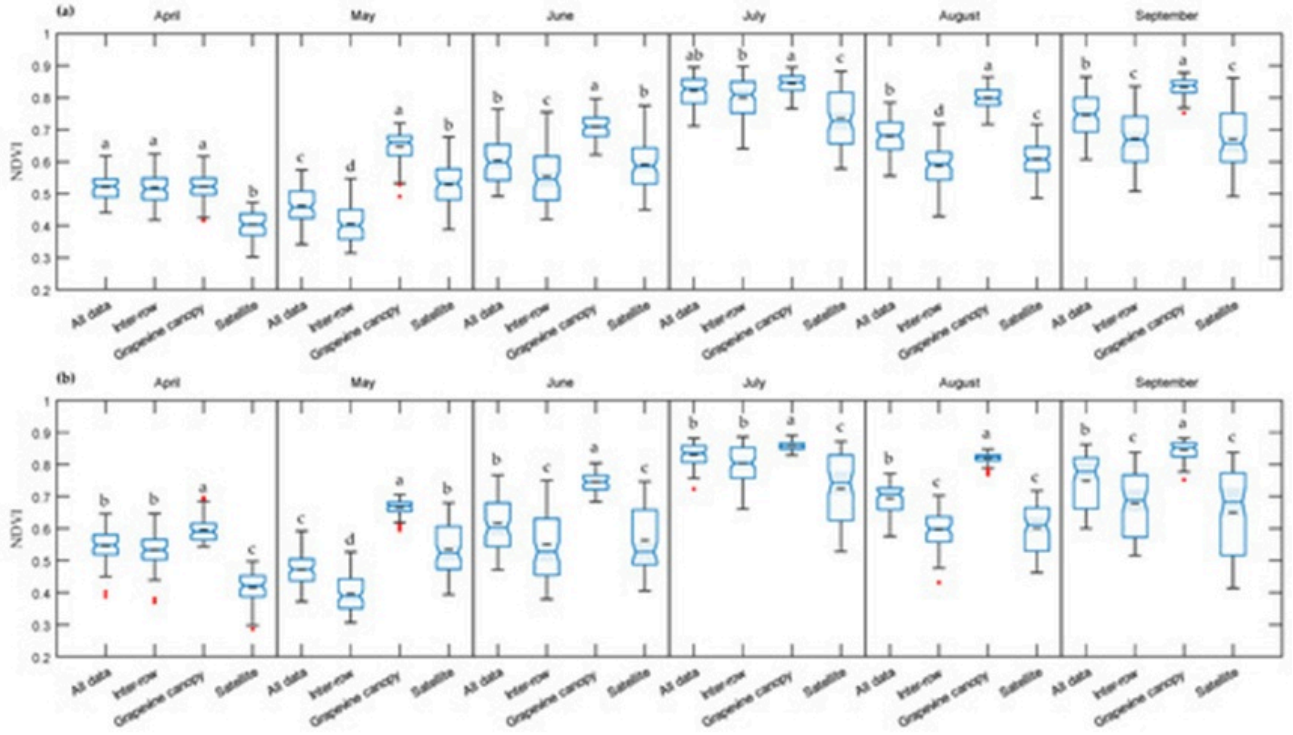


Figure 8. Boxplots representing the dispersion of the normalized difference vegetation index (NDVI) values obtained for the different scenarios from April to September 2021, for Plot A (a) and Plot B (b). The letters indicate whether there is a statistical difference between the scenarios at the 5% significance level for each month. The notches in each box represent the significance of the median. Box charts whose notches do not overlap have different medians at the 5% significance level (P-value < 0.05). The black line in each box represents the mean, and the red symbols represent outliers.

During April, grapevines remain in leaf development and therefore add limited soil coverage. Under these conditions, Plot A shows no statistical differences among scenarios, except for the satellite dataset ($P \geq 0.98$). Plot B, however, shows that the grapevine canopy-only strategy differs statistically from all others, not only in April but also throughout the year. All data and inter-row strategies lack statistical distinction ($P = 0.23$), yet both differ from satellite NDVI. The satellite dataset records its smallest NDVI in April. In May, during inflorescence emergence, every scenario differs statistically, ordered from highest to lowest: grapevine canopy, satellite, all data, then inter-row. Despite continuing canopy growth, inter-row zones still dominate the vineyard surface. Low inter-row NDVI likely lowered all-data and satellite figures, which cover the entire surface. In the flowering window (June), the gap between the grapevine canopy and all-data averages shrinks. Grapevine canopy differs from the remaining strategies in both plots. Plot A shows no distinction between all data and satellite ($P = 0.61$), though both exceed inter-row. In Plot B, the lowest readings are associated with inter-row and satellite ($P = 0.77$). In July, during fruit development, Plot A grapevine canopy matches all data ($P = 0.05$), and all data show no statistical gap from inter-row ($P = 0.06$). Plot B places the grapevine canopy highest, followed by all data and inter-row, which lack distinction ($P = 0.05$). Satellite yields the lowest NDVI in both plots.

August sees an overall average decline in NDVI. Vineyard vegetation controls applied between July and August, such as pruning and inter-row clearing, undoubtedly drove this drop. Reduced vigor hits inter-row hardest, directly influencing the full surface assessed by all data and satellite. Plot B data supports this, showing inter-row and satellite statistically identical ($P = 0.98$). Similar patterns appeared in June. In September (berry ripening), NDVI rises again, and the gap between grapevine canopy and other strategies persists, notably compared with inter-row and satellite, which show no distinction in Plot A ($P = 0.99$) or Plot B ($P = 0.20$).

© 2026 The Author(s). | Published by Agro Intelligence Research Press

Parallel examination addressed grapevine canopy area and volume from UAV sources **(Figure 9)**. The same broad NDVI average pattern holds across scenarios. Grapevine canopy area stays modest in the first three months of active vegetative growth. Canopy volume behaves similarly, depending directly on area and height. May sees inter-row area reductions of 51% in Plot A and 62% in Plot B. Peak canopy area and volume values arrive in July, the strongest vigor phase **(Figure 8)**. Pruning between July and August causes 18% canopy area loss and 19% volume loss in both plots. Inter-row vegetation after management shows similar declines: 19% in Plot A and 14% in Plot B. From August to September, the balance shifts toward greater grapevine canopy coverage and less inter-row herbaceous vegetation.

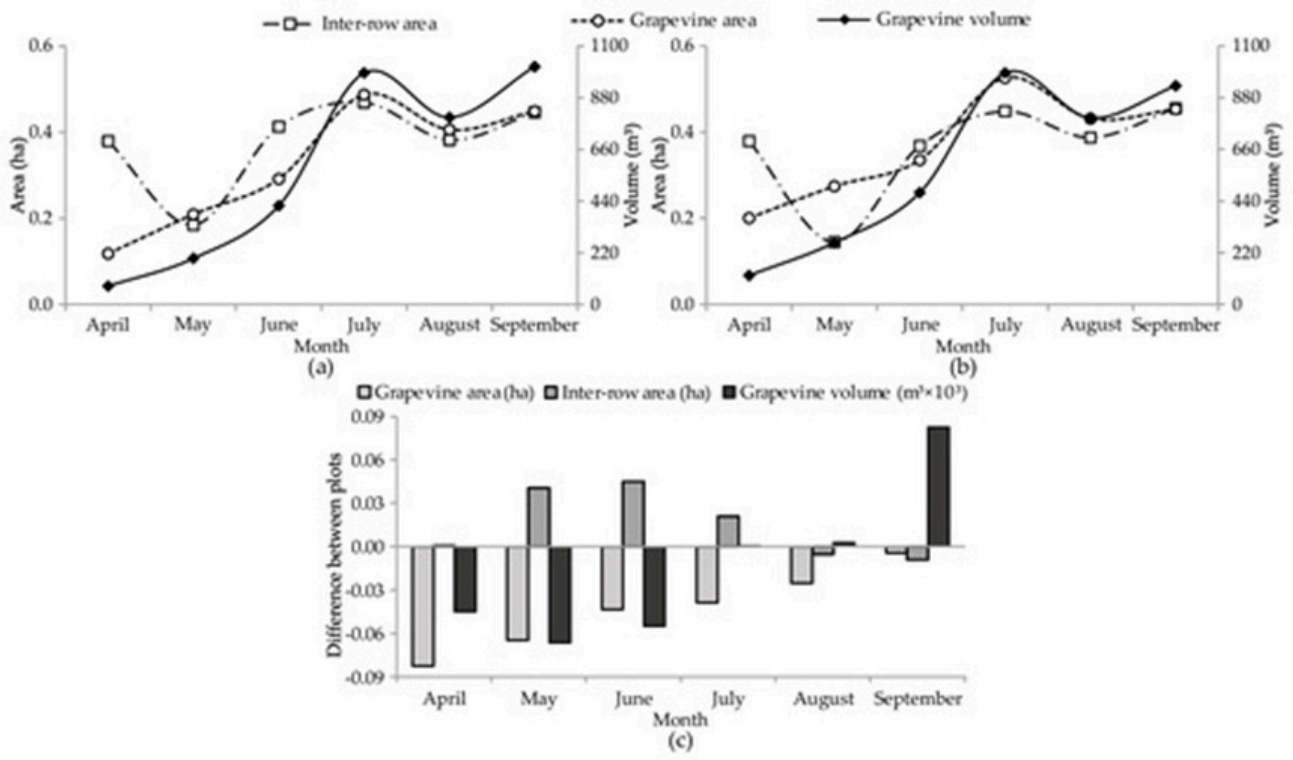


Figure 9. Total inter-row vegetation, grapevine canopy area, and grapevine volume for Plot A (cv. Sousão) (a), Plot B (cv. Sauvignon blanc) (b), and the difference in each parameter between Plot A and Plot B (c) for the evaluated period (April to September 2021).

These findings clearly demonstrate that Plot B maintains a larger grapevine canopy area than Plot A over the full period, with the difference most pronounced in April at 8%. The reduction trend eased in the following months: 6% in May, 4% in June, 3% in July and August, and below 1% in September. Early months show bigger differences that gradually shrink as grapevine vegetative structures expand. Plot B canopy volume exceeds Plot A from April to June. The difference narrows in July, then reverses so Plot A surpasses Plot B, reaching 82.62 m3ha−1 by September. Plot A also has more inter-row herbaceous vegetation from May to July than Plot B. Meanwhile, Plot B displays greater canopy volume and overall area coverage.

Data correlation

Figure 10 displays the straight-line relationships between predictor elements from UAV sources (full coverage, inter-row zones, and grapevine canopy) and the Sentinel-2 response element (satellite). Linear fit strength from April through September proves stronger overall in Plot A, particularly with grapevine canopy (R2 = 0.77), which surpassed full coverage (R2 = 0.72) and inter-row zones (R2 = 0.63). For Plot B, full coverage delivers the clearest performance, explaining 66% of NDVI variance within the linear model, ahead of inter-row zones (R2 = 0.59) and the grapevine canopy (R2 = 0.58). A joint review of both plots reveals that full coverage, inter-row zones, and grapevine canopy strategies

© 2026 The Author(s). | Published by Agro Intelligence Research Press

cannot capture all the variation in the response element. Even so, linear models built for the separate strategies and plots still explain at least 58% of the variance in satellite NDVI readings collected over the six months starting in April 2021.

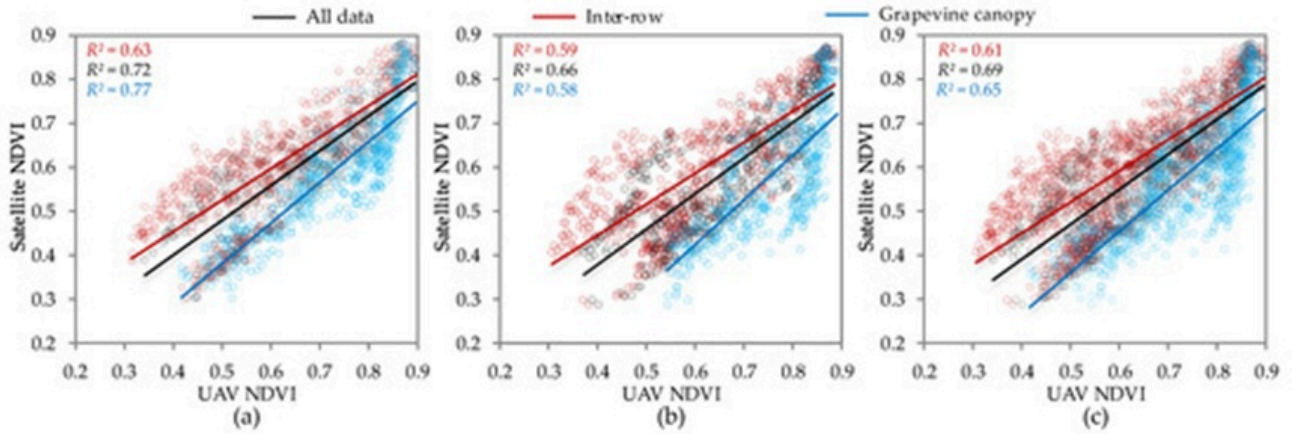


Figure 10. Linear correlation of the predictor variables (all data, inter-row, and grapevine canopy) for Plot A (a), Plot B (b), and for both plots (c), with the response variable (satellite) for the six months. Values refer to the normalized difference vegetation index (NDVI). All data, inter-row, and grapevine canopy values are obtained from unmanned aerial vehicle multi-spectral data, and satellite values are obtained from the Sentinel-2 multi-spectral instrument.

Across the entire six-month research window, grapevine canopy NDVI readings clarify a substantial portion of the variation in satellite-based records. Monthly breakdowns, however, produce different outcomes. **Table 2** demonstrates that full coverage and inter-row zone strategies better explain satellite-based NDVI variation than the grapevine canopy. Early vegetative growth features quite limited grapevine leaf coverage, restricted mainly to trunk surroundings. Species growing under vines, especially in inter-row zones during April, exert a major influence on NDVI readings, as they are the chief elements then. Beginning in May, grapevines build additional biomass while shoot expansion widens leaf coverage. This stage marks when grapevines begin to visibly contribute to total vineyard vigor.

Nevertheless, grapevine vegetative expansion remains confined within planting rows, without spanning the entire plot surface. Inter-row zones preserve steady patterns during the vineyard's complete growth cycle. Yet, periods of weak grapevine vegetative presence, mainly leaf development (April) and immediately after management actions (May), favor the inter-row zones strategy **(Figure 9)**. July marks the grapevine canopy at its highest development, leading to expected maximum vigor and thus a stronger correlation with Sentinel-2 NDVI readings. This appears to be an improved correlation for the grapevine canopy in Plot A. Plot B fails to match this, instead showing higher inter-row-zone correlation that better accounts for Sentinel-2 NDVI readings. All strategies register lower correlation during August. The following month shows a strong correlation between Sentinel-2 and both inter-row zones and the grapevine canopy, although full coverage outperforms them.

Table 2. Coefficient of determination (R2) obtained from the linear correlation of the predictor variables (derived from the unmanned aerial vehicle—UAV—inter-row, grapevine canopy, and all data approaches) with the normalized difference vegetation index (NDVI) values of the satellite (Sentinel-2): when using the NDVI values; when using the vegetation cover area associated with the grapevine canopy, herbaceous vegetation in inter-row areas (NDVI > 0.5), and all data, that represents the sum of the vegetation cover associated with the two previous categories; and the correlation with grapevine volume, ns: non-significant.

Plot	Scenario	Metric	April	May	June	July	August	September
A	Inter-row	Normalized difference vegetation index	0.78	0.88	0.66	0.66	0.30	0.81

© 2026 The Author(s). | Published by Agro Intelligence Research Press

A	Grapevine canopy	Normalized difference vegetation index	0.17	0.57	0.59	0.63	0.41	0.71
A	All data	Normalized difference vegetation index	0.78	0.87	0.63	0.66	0.49	0.84
B	Inter-row	Normalized difference vegetation index	0.73	0.74	0.78	0.79	0.24	0.92
B	Grapevine canopy	Normalized difference vegetation index	0.23	0.62	0.61	0.24	0.02	0.78
B	All data	Normalized difference vegetation index	0.79	0.87	0.77	0.75	0.55	0.93
A	Inter-row	Vegetation cover area	0.69	0.80	0.67	0.15	0.05	0.10
A	Grapevine canopy	Vegetation cover area	0.16	ns	0.06	0.19	0.47	0.69
A	All data	Vegetation cover area	0.56	0.84	0.61	0.14	0.42	0.42
B	Inter-row	Vegetation cover area	0.31	0.55	0.78	0.25	0.02	0.12
B	Grapevine canopy	Vegetation cover area	0.35	0.30	0.11	0.29	0.68	0.77
B	All data	Vegetation cover area	0.70	0.81	0.80	0.28	0.52	0.68
A	Grapevine canopy	Grapevine volume	0.19	0.01	0.08	0.26	0.42	0.73
B	Grapevine canopy	Grapevine volume	0.29	0.22	0.27	0.50	0.72	0.85

Examination of NDVI readings from UAV-based strategies versus Sentinel-2 NDVI **(Table 2)** confirms that full coverage explains Sentinel-2 NDVI readings most effectively by including the entire grapevine cultivation surface. Resolution differences carry minimal weight on overall patterns here. Inter-row zones form part of full coverage yet affect Sentinel-2 NDVI more strongly than the grapevine canopy. Coverage from both the grapevine canopy and inter-row vegetation appears to shape satellite-derived NDVI readings.

A deeper exploration of this connection involves correlational testing of satellite NDVI readings with inter-row vegetation, grapevine canopy, and full coverage (the sum of the first two). **Table 2** findings show that scenario coverage has a noticeable influence on satellite NDVI values. Grapevine canopy coverage also shows some correlation with satellite records during the ripening window, with August for Plot B and September for Plot A. This reverses the inter-row vegetation coverage pattern, which shows a strong correlation early (April, May, June), precisely when vine canopy area and volume remain small. Current work records grapevine canopy coverage between 12% and 49% of the crop surface in Plot A and 20% to 53% in Plot B. The lowest coverage occurs in April, while July brings the highest in both plots.

Table 2 also indicates that scenario coverage alone cannot fully explain variation in satellite NDVI readings across grapevine growth and maturation stages. July, for example, features grapevine canopy area and volume at higher levels than any other month **(Figure 9)**, yet both plots yield low correlation with satellite NDVI. Vine vigor arises from vegetative structure expansion that satellite records detect poorly at cycle start. Canopy coverage can affect this process, above all in ripening (August–September), owing to reduced variation and grapevine canopy dominance compared with other vegetation inside inter-row zones. Supporting evidence comes from testing the relationship between grapevine canopy volume and satellite NDVI. **Table 2** presents these values, showing that grapevine canopy volume influences satellite NDVI values from July onward in Plot B and from August onward in Plot A. Plot B displays a stronger correlation, especially before September. Plot B then holds maximum grapevine canopy area and volume, overtaken by Plot A only in September regarding volume alone **(Figure 9)**.

Multi-temporal analysis of the different approaches

Vineyard tracking across multiple dates in this research yielded notable outcomes at various levels. Phenological stage shifts are clearly evident in GDD accumulation **(Figure 4)** and remain closely tied to NDVI readings, matching prior observations by other researchers [50]. NDVI and GDD curves typically resemble each other as they track the annual

© 2026 The Author(s). | Published by Agro Intelligence Research Press

grapevine biological rhythm [51]. This research records the same patterns in both Sentinel-2 and UAV records. Phenological modeling **(Figure 4)** reveals that 2021 GDD accumulation exceeded the four-year average in the first four months. Understanding phenological phases remains critical when constructing reliable frameworks for NDVI readings sourced from satellite and UAV multi-spectral imagery. A multi-temporal review of strategies **(Figures 7 and 8)** clearly reveals varying vine growth behaviors over time. **Figure 2** illustrates that April–June experienced favorable precipitation, which surely promoted spontaneous vegetation growth ahead of grapevines [52]. Limited grapevine canopy area and volume nevertheless allowed stronger light reach into inter-row zones, mainly supporting sun-loving herbaceous species **(Figure 9)** [51]. Early-year lack of vine canopy left spontaneous inter-row vegetation as the sole indicator of plot vegetative vigor. These details offer substantial agronomic value. In the Northern Hemisphere, April is the optimal window for vineyard soil fertilization with higher applications, as vegetative vigor remains low [27]. Since inter-row vegetation typically receives at least one management treatment each year, records can also guide upcoming spontaneous vegetation management through mowing or tillage aimed at reducing water competition from permanent plants and reducing vineyard frost risk [53].

Higher average NDVI readings from UAV multi-spectral sources focused on the grapevine canopy stand out clearly. These readings differed statistically significantly from the remaining scenarios across nearly all stages of grapevine canopy expansion **(Figure 8)**. As a result, the plot segmentation technique used to separate clean grapevine canopy pixels from other vineyard components [37] emerges as a suitable method for capturing vigor specifically associated with the grapevine canopy. Indeed, relying solely on grapevine vigor is the only reliable way to prevent skewed assessments, particularly under cordon systems, where inter-row surfaces often host grass or other plants exposed to human activities such as pest management, disease treatment, or ground clearing [31].

NDVI responds heavily to vineyard surface layout, canopy design, and leaf positioning [54], meaning any modification within the vineyard directly alters plot vigor. Nevertheless, several subtle shifts within the vineyard plots remained undetectable in Sentinel-2 records **(Table 2)**. As an illustration, NDVI dropped for full coverage and inter-row strategies in May immediately following spontaneous vegetation trimming **(Figure 8)**, while a modest contraction in grapevine canopy coverage during June **(Figure 9)** after shoot alignment and training activities appeared solely in the UAV records. The higher spatial resolution of Sentinel-2 accounts for the elevated NDVI fluctuations observed **(Figure 8)**. Within any single pixel, an elevated share of undesired components beyond grapevine canopy coverage alone triggers this outcome in satellite imagery [23]. Spectral values within the images are influenced by boundaries, whereby pixels near the edges of the target zone mix with neighboring features such as trails, open ground, or varied vegetation forms, which can lower or raise pixel spectral readings [23, 30]. Sentinel-2 image resolution can pose a genuine barrier because it blocks the application of vegetation filtering techniques [7] comparable to the method adopted here. Conversely, Sentinel-2 time-series records successfully identify key vineyard operations, such as pruning, which are performed to regulate vigor, encourage secondary shoot formation, boost productive performance [27], and enhance plot consistency [55]. Detection of these shifts in satellite time series is driven by links between satellite NDVI and UAV-generated scenarios **(Figure 10)**. Agreement across the two platforms is supported by R2 figures exceeding 0.6 in over 78% of comparisons and remaining above 0.58 in every case. Khaliq *et al.* [31] examined cv. Nebbiolo vineyards in Piedmont (northwestern Italy); Pearson correlation (r) values between Sentinel-2 and UAV methods, similar to those employed here, also proved strong, exceeding 0.55. Further support for the potential of Sentinel-2 imagery for NDVI-based vigor description is provided by Devaux *et al.* [30].

Maximum vegetative expansion arrives in July **(Figures 8 and 9)**, aligning with documented grapevine patterns across the northern hemisphere [23, 30, 31, 56, 57]. This timing is not fixed, however, as it depends on vineyard genetic traits and yearly weather patterns [27]. Despite elevated vigor linked to grapevine canopy during July, correlations between grapevine canopy coverage and Sentinel-2 NDVI were lower. Canopy coverage expansion likely contributed to the heightened vigor differences within the plots. At this stage, grapevine leaves attain complete maturity [52] with expanded leaf surface. In contrast, secondary shoots emerge from primary shoots, bearing young leaves that consume photoassimilates, thereby affecting grapevine canopy reflectance and the resulting NDVI. UAV-based records can register

© 2026 The Author(s). | Published by Agro Intelligence Research Press

such canopy variations thanks to their fine resolution [7, 36], helping account for the weak correlation between grapevine canopy coverage and Sentinel-2 NDVI caused by the latter's coarser scale.

From July to August, rainwater exerted minimal effect on the soil **(Figure 2)**, indicating these were the months of highest water demand. The general vineyard-wide decline in NDVI registered in August is linked to rising average temperatures, a lack of rainfall, declining soil moisture, and insufficient water provision to plants [27, 52]. Puig-Sirera *et al.* [54] note that soil water shortage during the veraison stage (through August) can reduce photosynthetic function and lead to a decline in vegetative vigor. Leaf coverage contraction is a vine adaptation that limits water loss. In reality, zones supporting stronger vines often experience greater water stress, which can reduce both yield volume and quality [58]. Despite water limitations, grapevine canopy sustains higher vigor levels than herbaceous growth between rows, as visible in **Figure 8**. This outcome indicates that grapevine vigor is less affected by dry, warm conditions than herbaceous vegetation [52]. Even where variation existed within individual plants or rows, grapevine canopy coverage would fill row gaps [59] and, paired with absent inter-row vegetation, emerge as the dominant contributor to genuine vineyard plot vigor captured by Sentinel-2 records.

Dry conditions combined with human activities within the cultivated zone from July to August had direct effects on inter-row vegetation **(Figure 9)**. Pruning reduced total vigor across both examined plots and reduced canopy coverage to below 43% of the vineyard plot. Consequently, exposure between rows grew. Greater inter-row presence should therefore have strengthened its effect on Sentinel-2 NDVI value, yet this shift did not appear right away. Vigor decline **(Figure 8)** and inter-row herbaceous coverage falling below 39% of the plot **(Figure 9)** heightened environmental heterogeneity by increasing the mixing of components (e.g., exposed soil, stones, dry material), occupying 18% of the area. Likely, the pronounced inter-row variation identified from UAV multi-spectral records escaped satellite detection, clarifying the weak correlation between satellite NDVI values and the various strategies.

Grapevine canopy coverage and volume acquired greater importance in September, immediately following veraison, coinciding with a strengthened correlation between grapevine canopy and Sentinel-2 NDVI **(Table 2)**. By then, the vineyard has reached full maturity, with no substantial further changes, producing more consistent NDVI spatial patterns [54]. Still, Sentinel-2's reduced resolution suggests lower satellite values than UAV-derived scenarios [29]. This expectation did not hold consistently **(Figure 8)**. During May, Sentinel-2 NDVI readings for both plots surpassed UAV-based inter-row and full coverage NDVI, whereas in June and August, inter-row NDVI in Plot A also fell below Sentinel-2 levels. Reductions in inter-row NDVI values probably stemmed from plot-level operations such as herbaceous vegetation cutting.

Coefficients of determination calculated from May through September match existing literature [31, 37, 55]. Among the tested strategies, grapevine canopy shows the weakest association with Sentinel-2 NDVI, echoing findings from other researchers [55]. Grapevine canopy R2 values extended from 0.17 to 0.71 in Plot A and from 0.02 to 0.78 in Plot B **(Table 2)**. This spread appears meaningful beside R2 ranges reported by Pastonchi *et al.* [55] for cv. Sangiovese vineyard plots in Tuscany (Italy), spanning 0.53 to 0.80, and by Khaliq *et al.* [31] using correlation coefficient (r) with outcomes between 0.28 and 0.61. The current study covered a continuous six-month window from April onward, unlike Khaliq *et al.* [31], who focused on May, June, August, and September, and Pastonchi *et al.* [55], who examined June and August in 2017–2018 and August and September in 2019. For the UAV-based inter-row zones strategy, Plot A R2 ranged from 0.30 to 0.88, while Plot B ranged from 0.24 to 0.92. Apart from August, the remaining months in this research yielded higher R2 figures above 0.66. Khaliq *et al.* [31] noted comparable trends, with all r values exceeding 0.50 except in one plot. Lastly, full UAV-based data produced the most aligned outcomes, with the smallest variation in correlations, in Plot A (0.49 to 0.87) and Plot B (0.55 to 0.93). This mirrors Pastonchi *et al.* [55], with R2 ranging from 0.59 to 0.80, and Khaliq *et al.* [31], with r ranging from 0.55 to 0.72. When linking full data across both platforms, May and September delivered peak R2 values of 0.87-0.93, substantially above the findings of Matese *et al.* [37] for two cv. Cabernet Sauvignon plots in Italy where r values comparing UAV and RapidEye satellite data ranged from 0.29 to 0.80.

© 2026 The Author(s). | Published by Agro Intelligence Research Press

Associations identified here match patterns reported elsewhere [31, 55]. Still, noticeable gaps exist between the upper and lower extremes. May delivered the strongest NDVI associations through inter-row and full coverage strategies inside both plots. Plot A reached R2 = 0.88 for inter-row vegetation alone and 0.87 for complete UAV vineyard NDVI data, while Plot B recorded 0.74 for inter-row and 0.87 for full coverage. In the same timeframe, Khaliq *et al.* [31] reported r values ranging from 0.52 to 0.59 for inter-row zones and 0.60 to 0.64 for all data. **Table 2** indicates grapevine canopy R2 exceeded 0.50 in 67% of months reviewed for Plot A and 50% for Plot B. By comparison, Khaliq *et al.* [31] found only 17% of r values above 0.50 across three plots monitored over four months. Stronger coefficients here versus Khaliq *et al.* [31] probably arise from variations in processing methods, cultivation techniques, and plot vigor characteristics. Inter-row zones, which at times dominate the plot surface as noted earlier, correlate most closely with Sentinel-2 records among vineyard features. Their larger contribution makes Sentinel-2 detection easier, leading to consistent under-representation of grapevine canopy vigor throughout most of the active growth window.

A side-by-side comparison of the two plots revealed clear phenological differences between the red and white cultivars. Plot B maintained modestly elevated NDVI levels over Plot A when limited to the grapevine canopy for the full research duration **(Figure 7)**, despite uniform management, identical weather, and matching soil across sites. Comparetti and Silva [27] attributed vigor differences in cvs. Nero d'Avola and Syrah from Sicily (Italy) to inherit the genetic traits of each cultivar. Here cv. Sousão (Plot A) represents a red variety and cv. Sauvignon Blanc (Plot B) is a white cultivar; white cultivars typically mature earlier than red types [60]. GDD calculations confirm cv. Sauvignon Blanc advances phenological stages with fewer heat units than cv. Sousão [46, 61]. This accounts for the larger grapevine canopy coverage and volume in Plot B during the early months **(Figure 9)**, as well as its faster maturation, shown by slower growth alongside rising canopy volume in cv. Sousão.

Benefits of synergistic or individual use of sentinel-2 and UAV multi-spectral data

Findings from this work, backed by further literature [27, 29-31, 37, 55], confirm that Sentinel-2 and UAV multi-spectral records both track temporal changes in vineyards across grapevine vegetative phenological phases. Situations with little or no grapevine vegetation—senescence (following leaf drop), budburst, and initial leaf expansion—yield high correlations in **Table 2**. Sentinel-2 MSI records therefore support broad vineyard vigor monitoring by drawing on spectral signals from spontaneous inter-row vegetation. This aids in scheduling and executing plot-level actions and helps address soil nutrient gaps. Sentinel-2 likewise performs well in fruit development and ripening windows. A more uniform vegetation layout then enables accurate grapevine depiction [37], which is suitable for Sentinel-2 evaluation. These points matter greatly because they enable wide-area, low- or no-cost data use. Sentinel-2 MSI thus becomes ideal for regional-scale vineyard spatial variation assessment [30]. UAVs can match coverage and timing but demand extra effort and markedly higher costs at large scales [37], requiring staff (at least two), repeated missions, multiple workdays, or fleets of UAVs, spare batteries, and processing/storage systems [62, 63].

Growers with field experience can use Sentinel-2 MSI data to monitor overall plot evolution over time. Main phenological shifts and human-induced changes, such as pruning, are clearly captured by Sentinel-2. Yet statistical tests show that UAV data offer better precision for grapevine-specific traits than Sentinel-2, particularly after plot management and at peak vegetative expansion, when canopy differences intensify. Sentinel-2's modest resolution makes separating soil and crop signals difficult in plots where grapevines cover under 25% of the surface [7]. UAV records readily isolate the grapevine canopy from other features.

UAV records suit the full vegetative cycle [56], though they add limited value in the earliest stages. Different sensors expand UAV options for specialized tasks. RGB imagery works for vegetation mapping or classification [64] to measure grapevine and inter-row extents [56]. Interventions receive tracking, but vigor impacts—as studied here—need multi-spectral input. Multi-spectral records yield vineyard biophysical metrics and vigor maps free of non-grapevine areas [48, 57], which are impossible with Sentinel-2 MSI. Inter-row mapping inside vineyards helps identify invasive plants among ground covers [65]. High UAV resolution further enables the extraction of individual grapevine structural and biophysical

© 2026 The Author(s). | Published by Agro Intelligence Research Press

traits, which are vital for detailed analysis [59, 66, 67]. In precision viticulture, plant-level work enables automatic detection of missing vines for disease spotting [68, 69] and for tracking water stress [70, 71].

Conclusion

This research tests an affordable remote sensing strategy with strong potential to advance precision viticulture and production efficiency, delivering uniform high-quality output and greater profitability. Emphasis lies on medium-resolution imagery, often sidelined beside high-resolution UAV sources, yet useful for monitoring grapevine condition and management to better follow plant development and evaluate performance over time. Sentinel-2 MSI records and UAV-derived data both contribute meaningfully to vigor control and vineyard variation detection. Best results in precision viticulture come from merging the two platforms. Sentinel-2 offers the most cost-effective approach for a general vegetation overview of any vineyard plot. When goals require surface element separation via filtering and pure pixel data, or localized plant-scale actions, UAV records prove superior.

A comparison of Sentinel-2 and UAV performance for phenological stage identification shows that average NDVI values remained closely aligned after standardization to a common resolution. The largest divergences followed plot-level farming operations. Plot segmentation highlights inter-row elements occasionally dominating Sentinel-2 NDVI. Inter-row influence on Sentinel-2 NDVI weakens when inter-row variation drops, improving Sentinel-2 detection of grapevine canopy vigor. For cordon systems, lowering between-row heterogeneity appears promising for better Sentinel-2 results. More trials are required to verify these observations. Future studies should test various inter-row setups, including different cover crops, soil practices, and aggregate surface covers.

Acknowledgements

None

Conflict of interest

None

Financial support

We acknowledge the CoaClimateRisk project (COA/CAC/0030/2019) and the projects UIDB/04033/2020 and LA/P/0126/2020, both supported by National Funds by FCT—Portuguese Foundation for Science and Technology and the project “DATI—Digital Agriculture Technologies for Irrigation efficiency”, PRIMA—Partnership for Research and Innovation in the Mediterranean Area, (Research and Innovation activities), financed by the states participating in the PRIMA partnership and by the European Union through Horizon 2020. H.F. thanks the FCT for CEECIND/00447/2017 and 2022.02317.CEECIND. We would also like to thank “Fundação da Casa de Mateus” for its collaboration in making the vineyard’s facilities and weather data available for this research work.

Ethics statement

None

Received: 05 Oct 2024 Revised: 10 Dec 2024 Accepted: 27 Dec 2024
Published online: 25 November 2026

© 2026 The Author(s). | Published by Agro Intelligence Research Press

Rights and permissions

Open Access The author(s) retain copyright. This article is licensed under the Creative Commons Attribution-NonCommercial-ShareAlike 4.0 International License. It may be shared and adapted for non-commercial purposes with appropriate attribution, an indication of changes, and distribution of adaptations under the same license. Third-party material may be subject to separate terms identified in its credit line. View the license at https://creativecommons.org/licenses/by-nc-sa/4.0/.

References

1. Khosla R. Precision Agriculture: Challenges and Opportunities in a Flat World. In Proceedings of the 2010 19th World Congress of Soil Science, Soil Solutions for a Changing World, Brisbane, Australia; 2010. p. 26–8.

2. Pierce FJ, Robert PC, Mangold G. Site Specific Management: The Pros, the Cons, and the Realities. In: Proceedings of the Integrated Crop Management Conference, Ames, IA, USA;1994; p. 11934214.

3. Santesteban LG. Precision Viticulture and Advanced Analytics. A Short Review. Food Chem. 2019;279:58–62.

4. Matese A, Di Gennaro SF. Technology in Precision Viticulture: A State of the Art Review. Int J Wine Res. 2015;69.

5. Manson SM, Bonsal DB, Kernik M, Lambin EF. Geographic Information Systems and Remote Sensing. In: International Encyclopedia of the Social and Behavioral Sciences. 2nd ed; Wright JD, Ed; Elsevier: Oxford, UK; 2015. p. 64–8. ISBN 978-0-08-097087-5.

6. Viscarra Rossel RA, Adamchuk VI, Sudduth KA, McKenzie NJ, Lobsey C. Proximal Soil Sensing: An Effective Approach for Soil Measurements in Space and Time. Adv Agron. 2011;113:243–91.

7. Brook A, De Micco V, Battipaglia G, Erbaggio A, Ludeno G, Catapano I, et al. A Smart Multiple Spatial and Temporal Resolution System to Support Precision Agriculture from Satellite Images: Proof of Concept on Aglianico Vineyard. Remote Sens Environ. 2020;240:111679.

8. Hall A, Lamb DW, Holzapfel B, Louis J. Optical Remote Sensing Applications in Viticulture—A Review. Aust J Grape Wine Res. 2002;8:36–47.

9. Gatti M, Dosso P, Maurino M, Merli MC, Bernizzoni F, José Pirez F, et al. MECS-VINE®: A New Proximal Sensor for Segmented Mapping of Vigor and Yield Parameters on Vineyard Rows. Sensors. 2016;16:2009.

10. Green EP, Edwards AJ, Eds. Remote Sensing Handbook for Tropical Coastal Management. Coastal Management Sourcebooks. Paris, France: Unesco Pub; 2000. ISBN 978-92-3-103736-8.

11. Alvarez-Vanhard E, Corpetti T, Houet T. UAV and Satellite Synergies for Optical Remote Sensing Applications: A Literature Review. Sci Remote Sens. 2021;3:100019.

12. Mulla DJ. Twenty Five Years of Remote Sensing in Precision Agriculture: Key Advances and Remaining Knowledge Gaps. Biosyst Eng. 2013;114:358–71.

13. Sishodia RP, Ray RL, Singh SK. Applications of Remote Sensing in Precision Agriculture: A Review. Remote Sens. 2020;12:3136.

14. Yang G, Liu J, Zhao C, Li Z, Huang Y, Yu H, et al. Unmanned Aerial Vehicle Remote Sensing for Field-Based Crop Phenotyping: Current Status and Perspectives. Front Plant Sci. 2017;8:1111.

15. Katsigiannis P, Galanis G, Dimitrakos A, Tsakiridis N, Kalopesas C, Alexandridis T, et al. Fusion of Spatio-Temporal UAV and Proximal Sensing Data for an Agricultural Decision Support System. In: Proceedings of the Fourth International Conference on

Remote Sensing and Geoinformation of the Environment, Paphos, Cyprus, 2016; Themistocleous K, Hadjimitsis DG, Michaelides S, Papadavid G, Eds. 2016; 9688.

16. Gasmi A, Masse A, Ducrot D, Zouari H. Télédétection et photogrammétrie pour l'étude de la dynamique de l'occupation du sol dans le bassin versant de l'oued Chiba (Cap-Bon, Tunisie). Rev Fr Photogrammétrie Télédétection. 2017:43–51.

17. Romero M, Luo Y, Su B, Fuentes S. Vineyard Water Status Estimation Using Multi-spectral Imagery from an UAV Platform and Machine Learning Algorithms for Irrigation Scheduling Management. Comput Electron Agric. 2018;147:109–17.

18. Hatfield JL, Prueger JH, Sauer TJ, Dold C, O'Brien P, Wacha K. Applications of Vegetative Indices from Remote Sensing to Agriculture: Past and Future. Inventions. 2019;4:71.

19. Giovos R, Tassopoulos D, Kalivas D, Lougkos N, Priovolou A. Remote Sensing Vegetation Indices in Viticulture: A Critical Review. Agriculture. 2021;11:457.

20. Rouse W, Haas RH, Schell JA, Deering DW. Monitoring Vegetation Systems in The Great Plains With ERTS. NASA Spec Publ. 1974;351:309–17.

21. Xue J, Su B. Significant Remote Sensing Vegetation Indices: A Review of Developments and Applications. J Sens. 2017;2017:e1353691.

22. Priori S, Martini E, Andrenelli MC, Magini S, Agnelli AE, Bucelli P, et al. Improving Wine Quality through Harvest Zoning and Combined Use of Remote and Soil Proximal Sensing. Soil Sci Soc Am J. 2013;77:1338–48.

23. Campos J, García-Ruíz F, Gil E. Assessment of Vineyard Canopy Characteristics from Vigour Maps Obtained Using UAV and Satellite Imagery. Sensors. 2021;21:2363.

24. Ferrer M, Echeverría G, Pereyra G, Gonzalez-Neves G, Pan D, Mirás-Avalos JM. Mapping vineyard vigor using airborne remote sensing: relations with yield, berry composition and sanitary status under humid climate conditions. Precis Agric. 2020;21:178–97.

25. Cogato A, Meggio F, Collins C, Marinello F. Medium-Resolution multi-spectral data from sentinel-2 to assess the damage and the recovery time of late frost on vineyards. Remote Sens. 2020;12:1896.

26. Cogato A, Pagay V, Marinello F, Meggio F, Grace P, De Antoni Migliorati M. Assessing the feasibility of using sentinel-2 imagery to quantify the impact of heatwaves on irrigated vineyards. Remote Sens. 2019;11:2869.

27. Comparetti A, Marques da Silva JR. Use of sentinel-2 satellite for spatially variable rate fertiliser management in a sicilian vineyard. Sustainability. 2022;14:1688.

28. Esteves C, Fangueiro D, Braga RP, Martins M, Botelho M, Ribeiro H. Assessing the Contribution of ECa and NDVI in the Delineation of Management Zones in a Vineyard. Agronomy. 2022;12:1331.

29. Bollas N, Kokinou E, Polychronos V. Comparison of sentinel-2 and uav multi-spectral data for use in precision agriculture: an application from northern greece. Drones. 2021;5:35.

30. Devaux N, Crestey T, Leroux C, Tisseyre B. Potential of sentinel-2 satellite images to monitor vine fields grown at a territorial scale. OENO One. 2019;53.

31. Khaliq A, Comba L, Biglia A, Ricauda Aimonino D, Chiaberge M, Gay P. Comparison of satellite and uav-based multi-spectral imagery for vineyard variability assessment. Remote Sens. 2019;11:436.

32. Hubbard SS, Schmutz M, Balde A, Falco N, Peruzzo L, Dafflon B, et al. Estimation of soil classes and their relationship to grapevine vigor in a bordeaux vineyard: advancing the practical joint use of electromagnetic induction (emi) and ndvi datasets for precision viticulture. Precis Agric. 2021;22:1353–76.

© 2026 The Author(s). | Published by Agro Intelligence Research Press

33. Di Gennaro SF, Dainelli R, Palliotti A, Toscano P, Matese A. Sentinel-2 validation for spatial variability assessment in overhead trellis system viticulture versus uav and agronomic data. Remote Sens. 2019;11:2573.

34. Müllerová J, Brůna J, Bartaloš T, Dvořák P, Vítková M, Pyšek P. Timing is important: unmanned aircraft vs. satellite imagery in plant invasion monitoring. Front Plant Sci. 2017;8:887.

35. Messina G, Peña JM, Vizzari M, Modica G. A Comparison of UAV and Satellites Multi-spectral Imagery in Monitoring Onion Crop. An Application in the 'Cipolla Rossa Di Tropea' (Italy). Remote Sens. 2020;12:3424.

36. Jain K, Pandey A. Calibration of satellite imagery with multi-spectral uav imagery. J Indian Soc Remote Sens. 2021;49:479–90.

37. Matese A, Toscano P, Di Gennaro SF, Genesio L, Vaccari FP, Primicerio J, et al. Intercomparison of UAV, aircraft and satellite remote sensing platforms for precision viticulture. Remote Sens. 2015;7:2971–90.

38. Lorenz DH, Eichhorn KW, Bleiholder H, Klose R, Meier U, Weber E. Growth stages of the grapevine: phenological growth stages of the grapevine (vitis vinifera l. ssp. vinifera)—codes and descriptions according to the extended bbch scale. Aust J Grape Wine Res. 1995;1:100–3.

39. Drusch M, Del Bello U, Carlier S, Colin O, Fernandez V, Gascon F, et al. Sentinel-2: esa's optical high-resolution mission for gmes operational services. Remote Sens Environ. 2012;120:25–36.

40. Main-Knorn M, Pflug B, Louis J, Debaecker V, Müller-Wilm U, Gascon F. Sen2Cor for Sentinel-2. In: Proceedings of the Image and Signal Processing for Remote Sensing XXIII, Warsaw, Poland; 2017; 10427: 37–48.

41. McMaster GS, Wilhelm WW. growing degree-days: one equation, two interpretations. Agric For Meteorol. 1997;87:291–300.

42. Winkler AJ. General Viticulture; University of California Press: Berkeley, CA, USA, 1974.

43. Amerine MA, Winkler AJ. Composition and quality of musts and wines of california grapes. Hilgardia. 1944;15:493–675.

44. Meier U. Growth Stages of Mono- and Dicotyledonous Plants: BBCH Monograph; Open Agrar Repositorium: Quedlinburg, Germany, 2018.

45. Ortega-Farias S, Riveros-Burgos C. Modeling phenology of four grapevine cultivars (vitis vinifera l.) in mediterranean climate conditions. Sci Hortic. 2019;250:38–44.

46. Lopes J, Eiras-Dias J, Abreu F, Clímaco P, Cunha JP, Silvestre J. Exigências térmicas, duração e precocidade de estados fenológicos de castas da colecção ampelográfica nacional. Ciênc E Téc Vitivinícola. 2007;23:61–71.

47. Di Gennaro SF, Matese A. Evaluation of novel precision viticulture tool for canopy biomass estimation and missing plant detection based on 2.5d and 3d approaches using rgb images acquired by uav platform. Plant Methods. 2020;16:91.

48. Duarte L, Teodoro AC, Sousa JJ, Pádua L. QVigourMap: A gis open source application for the creation of canopy vigour maps. Agronomy. 2021;11:952.

49. Tukey JW. Comparing Individual Means in the Analysis of Variance. Biometrics. 1949;5:99–114.

50. de Beurs KM, Henebry GM. Land surface phenology, climatic variation, and institutional change: analyzing agricultural land cover change in kazakhstan. Remote Sens Environ. 2004;89:497–509.

51. Borgogno-Mondino E, de Palma L, Novello V. Investigating sentinel-2 multi-spectral imagery efficiency in describing spectral response of vineyards covered with plastic sheets. Agronomy. 2020;10:1909.

© 2026 The Author(s). | Published by Agro Intelligence Research Press

52. Tezza L, Vendrame N, Pitacco A. Disentangling the carbon budget of a vineyard: the role of soil management. Agric Ecosyst Environ. 2019;272:52–62.

53. Magalhães N. Tratado De Viticultura: A Videira, A Vinha E O “Terroir”. 2nd ed. Lisboa, Portugal: Esfera Poética; 2015. ISBN: 978-989-98207-3-9.

54. Puig-Sirera À, Antichi D, Warren Raffa D, Rallo G. Application of remote sensing techniques to discriminate the effect of different soil management treatments over rainfed vineyards in chianti terroir. Remote Sens. 2021;13:716.

55. Pastonchi L, Gennaro SFD, Toscano P, Matese A. Comparison between satellite and ground data with uav-based information to analyse vineyard spatio-temporal variability. OENO One. 2020;54:919–34.

56. Pádua L, Marques P, Hruška J, Adão T, Peres E, Morais R, et al. Multi-temporal vineyard monitoring through UAV-based RGB imagery. Remote Sens. 2018;10:1907.

57. Pádua L, Marques P, Adão T, Guimarães N, Sousa A, Peres E, et al. Vineyard variability analysis through UAV-based vigour maps to assess climate change impacts. Agronomy. 2019;9:581.

58. Rey-Caramés C, Diago MP, Martín MP, Lobo A, Tardaguila J. Using RPAS multi-spectral imagery to characterise vigour, leaf development, yield components and berry composition variability within a vineyard. Remote Sens. 2015;7:14458-81.

59. Pádua L, Adão T, Sousa A, Peres E, Sousa JJ. Individual grapevine analysis in a multi-temporal context using UAV-based multi-sensor imagery. Remote Sens. 2020;12:139.

60. Kliewer WM. Free amino acids and other nitrogenous fractions in wine grapes. J Food Sci. 1970;35:17-21.

61. Van Leeuwen C, Garnier C, Agut C, Baculat B, Barbeau G, Besnard E, et al. Heat Requirements for Grapevine Varieties Is Essential Information to Adapt Plant Material in a Changing Climate; Food and Agriculture Organization: Rome, Italy, 2008.

62. Fernández-Guisuraga JM, Sanz-Ablanedo E, Suárez-Seoane S, Calvo L. Using unmanned aerial vehicles in postfire vegetation survey campaigns through large and heterogeneous areas: Opportunities and challenges. Sensors (Basel). 2018;18:586.

63. Pádua L, Guimarães N, Adão T, Sousa A, Peres E, Sousa JJ. Effectiveness of Sentinel-2 in multi-temporal post-fire monitoring when compared with UAV imagery. ISPRS Int J Geo-Inf. 2020;9:225.

64. Pádua L, Matese A, Di Gennaro SF, Morais R, Peres E, Sousa JJ. Vineyard classification using OBIA on UAV-based RGB and multi-spectral data: A case study in different wine regions. Comput Electron Agric. 2022;196:106905.

65. de Castro AI, Peña JM, Torres-Sánchez J, Jiménez-Brenes FM, Valencia-Gredilla F, Recasens J, et al. Mapping Cynodon dactylon infesting cover crops with an automatic decision tree-OBIA procedure and UAV imagery for precision viticulture. Remote Sens. 2020;12:56.

66. Jurado JM, Pádua L, Feito FR, Sousa JJ. Automatic grapevine trunk detection on UAV-based point cloud. Remote Sens. 2020;12:3043.

67. de Castro AI, Jiménez-Brenes FM, Torres-Sánchez J, Peña JM, Borra-Serrano I, López-Granados F. 3-D characterization of vineyards using a novel UAV imagery-based OBIA procedure for precision viticulture applications. Remote Sens. 2018;10:584.

68. Gennaro SFD, Battiston E, Marco SD, Facini O, Matese A, Nocentini M, et al. Unmanned aerial vehicle (UAV)-based remote sensing to monitor grapevine leaf stripe disease within a vineyard affected by Esca complex. Phytopathol Mediterr. 2016;55:262-75.

69. Albetis J, Jacquin A, Goulard M, Poilvé H, Rousseau J, Clenet H, et al. On the potentiality of UAV multi-spectral imagery to detect Flavescence dorée and grapevine trunk diseases. Remote Sens. 2019;11:23.

© 2026 The Author(s). | Published by Agro Intelligence Research Press

70. Soubry I, Patias P, Tsioukas V. Monitoring vineyards with UAV and multi-sensors for the assessment of water stress and grape maturity. J Unmanned Veh Syst. 2017;5:37-50.

71. Pádua L, Bernardo S, Dinis LT, Correia C, Moutinho-Pereira J, Sousa JJ. The efficiency of foliar kaolin spray assessed through UAV-based thermal infrared imagery. Remote Sens. 2022;14:4019.

© 2026 The Author(s). | Published by Agro Intelligence Research Press